Growth of ordered domains in a highly anisotropic two-dimensional system

O. M. Braun
Institute of Physics, Ukrainian Academy of Sciences, 46 Science Avenue, UA-252022 Kiev, Ukraine
and Laboratoire de Physique, Ecole Normale Supérieure de Lyon, 46 Allée d'Italie, 69364 Lyon Cédex 07, France

M. V. Paliy
Institute of Physics, Ukrainian Academy of Sciences, 46 Science Avenue, UA-252022 Kiev, Ukraine

M. Peyrard
Laboratoire de Physique, Ecole Normale Supérieure de Lyon, 46 Allée d'Italie, 69364 Lyon Cédex 07, France
(Received 29 May 1996; revised manuscript received 13 September 1996)

We introduce and study a lattice-gas model characterized by a strong anisotropy of the atomic mobility in different directions. The kinetics of the model is investigated by two methods, Monte Carlo simulation of the lattice-gas model and numerical solution of mean-field kinetic equations. The growth kinetics of the $p(2\times2)$ rarefied ordered structure at low temperature is shown to exhibit a hierarchy of growth rates owing to different evolution of the components of the $p(2\times2)$ phase order parameter. The rate of growth increases when the concentration is decreased below the stoichiometric value. Specific kinetics of the jump-anisotropic model and the effective repulsion between ordered domains result in an unusual evolution of the concentration gradient versus time. The model is applied to describe peculiar experimental results on surface diffusion of Li atoms adsorbed on furrowed single-crystal-plane Mo (112). [S0163-1829(97)04707-3]

I. INTRODUCTION

The growth of ordered domains in a system exhibiting a phase transition at a temperature T_c for the case of rapid quench from $T>T_c$ to $T<T_c$, is a very interesting problem (see Ref. 1 and references therein). Late-stage growth kinetics was found to exhibit self-similar temporal behavior and universality.[1] That is, it is expected that the system has a single characteristic length $R(t)$ associated with the average domain or island size, which grows asymptotically with time according to a power law

$$R(t)\propto t^z, t\to\infty, \tag{1}$$

where z is the *growth exponent*. The pair-correlation function $C(r,t)=\langle\phi(r,t)\phi(0,t)\rangle$ of the order parameter $\phi(r,t)$ and the structure factor $S(k,t)$ [$S(k,t)$ is the Fourier transform of $C(r,t)$] have to follow the scaling forms $C(r,t)=f(r/R(t))$, $S(k,t)=R^d(t)g(kR(t))$, where d is the spatial dimensionality of the system, and f and g are universal *scaling functions*.

The value of the growth exponent z depends, in particular, on the existence of the conservation law for the order parameter ϕ. That is, for the case of a nonconserved order parameter, the growth is governed by the curvature-driven motion of walls between ordered domains, which leads to the Lifshitz-Allen-Cahn (Refs. 2 and 3) growth law $R(t)\propto t^{1/2}$ at $t\to\infty$. When the order parameter is conserved, it is assumed that the basic mechanism for growth is the long-range diffusion of the order parameter through ordered regions from the interfaces characterized by a higher curvature to those with a lower curvature. Such a mechanism impedes the growth significantly, and results in the Lifshitz-Slyozov (Refs. 4 and 5) growth law $R(t)\propto t^{1/3}$. For the simplest case of a *scalar* order parameter ϕ these statements have been extensively checked by numerical solution of mean-field kinetic equations for the order parameter,[1,6] and by Monte Carlo simulation of various Ising-like (lattice-gas) models with nearest-neighbor (NN) interatomic interactions.[1,5,7]

In real physical systems the interatomic interaction is not reduced to the interaction of NN's only. In particular, in submonolayer adsorbed films the interaction may be anisotropic, and it may oscillate with interatomic distance.[8] Systems with competing interactions usually have a number of different stable and metastable phases. In addition, the ordered structure may be p-fold degenerated with $p>2$. For example, the O-W (110) adsystem, which can be described by the lattice-gas model with repulsion of the NN's and nex-NN's, has a fourfold-degenerated $p(2\times1)$-ordered phase.[9] Such systems are described by a *vector* order parameter. For instance, the order parameter $\vec{\phi}$ of the $p(2\times1)$ structure has two components $\vec{\phi}\equiv(\phi_1,\phi_2)$, which may be chosen as linear combinations of sublattice concentrations.[9] This order parameter is not conserved during system evolution. The conservation of the total concentration, nevertheless, impedes the growth as was shown by Sadiq and Binder,[9] who found $z\approx1/2$ for nonconserved concentration, and $z\approx1/3$ for the conserved concentration case. This slowing down of the growth may be attributed to an excess of atomic density contained in the walls between the domains,[9] that may be important for the systems with $p\geqslant3$.

Further complication arises for tricritical systems, where an ordered structure may coexist with another phase of different density (for instance, with the disordered lattice-gas phase). Conserved concentration in such a system was shown to impede the system dynamics and lead to the Lifshits-Slyozov growth law for the nonconserved parameter of the ordered phase.[10]

Another important generalization of the lattice-gas model involves the system anisotropy. The anisotropy of interatomic interaction results in the anisotropy of shape of growing domains as was shown by Ala-Nissilä Gunton, and Kaski.[11] Poulsen *et al.*[12] studied ordering dynamics in the *locally anisotropic two-dimensional lattice-gas model* introduced by Wille, Bevera, and de Fontaine,[13] to describe ordering processes in high-T_c superconductor $YBa_2Cu_3O_{7-\delta}$. It was found[12] that, in this model, where anisotropy of energetic parameters leads to quasi-one-dimensional effects in the ordering dynamics, two oxygen structures, the so-called ortho-I and ortho-II phases, obey growth laws with different exponents $z=\frac{1}{2}$ and $z=\frac{1}{3}$ correspondingly, in spite of the fact that both phases are characterized by the nonconserved order parameters. The slowing down of the ortho-II phase dynamics was explained[12] similarly to the Sadiq-Binder arguments mentioned above. That is, the excess or deficit of local oxygen density in domain walls result in long-range diffusion in the ordering process, and hence leads to the Lifshits-Slyozov growth law.

However, anisotropic systems may be characterized not only by the interaction anisotropy, but also by the anisotropy of probabilities of atomic jumps in different directions. Such a jump anisotropy does not modify the phase diagram of the system, but it might drastically modify the kinetics of a phase transition for the complicated lattice-gas model, where the ordered phase corresponds to a degenerated rarefied structure. *The aim of the present work is to study the effect of jump anisotropy on the growth of a rarefied phase.* We investigate the extreme case of the jump-anisotropic model, namely, the model where atomic jumps are allowed in a single direction only. One-dimensional mobility of atoms was found to exist in submonolayer films adsorbed on furrowed crystal surfaces such as the (112) surface of the fcc crystal or the (110) surface of the bcc crystal.[8,14] We use two basic approaches to investigate the model kinetics, Monte Carlo simulation (a part of these results has been published in Ref. 15) and a numerical solution of kinetic equations of the corresponding mean-field model. We show that growth kinetics of a rarefied ordered structure, as well as the evolution of an initial concentration gradient in the model of anisotropic jumps differ drastically from the case of the analogous but jump-isotropic model.

The paper is organized as follows. The model is described in Sec. II. We discuss the phenomenological approach to the problem in Sec. III. The temporal evolution of the homogeneous initial state is studied in Sec. IV: in Sec. IV A we briefly illustrate the behavior of the jump isotropic variant of the model, and the simulation results for the stoichiometric coverage in the jump anisotropic model are presented in Sec. IV B. The dependence of the growth rate on the atomic concentration is investigated in Sec. IV C. Section V is devoted to the system evolution in the case of nonhomogeneous initial state. Finally, Sec. VI concludes the paper with a discussion of a possible manifestation of the observed peculiar behavior of the jump-anisotropic model in surface diffusion on a macroscopic scale.

II. MODEL

We study a two-dimensional (2D) square lattice-gas model with a fixed atomic concentration characterized by the coverage $\theta=\mathcal{N}/\mathcal{M}$, where $\mathcal{N}$ is the number of atoms and $\mathcal{M}$ is the number of lattice sites. To obtain a rarefied ordered structure, we take into account the atomic interactions up to third neighbors with the energies $\varepsilon_1,\varepsilon_2$, and ε_3 for the nearest, next-nearest, and third neighbors, respectively, and assume a *repulsion* of nearest and next-nearest neighbors and an *attraction* of third neighbors. For this choice of interactions the low-coverage ordered phase for $\theta\leqslant\frac{1}{4}$ corresponds to the fourfold-degenerated $p(2\times2)$ structure, and with decreasing temperature the system exhibits a first-order phase transition to this phase. At higher coverages, $\frac{1}{4}<\theta<\frac{1}{2}$ (recall that the model has the atom-vacancy symmetry owing to pairwise character of interactions), the ordered phase has $p(2\times1)$ or $c(2\times2)$ structure depending on the ratio of energies ε_1 and ε_2. In the present work, however, we restrict our analysis to the low-coverage region $\theta\leqslant\frac{1}{4}$ only.

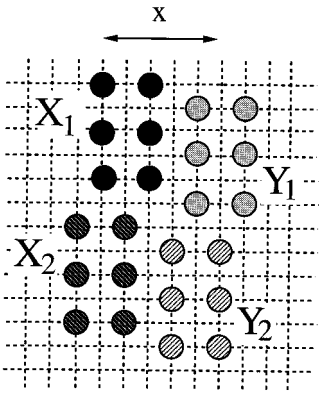

FIG. 1. Four translational types of the $p(2\times2)$ domains in the model under study. The direction of atomic jumps x for the jump-anisotropic case is indicated with arrows.

For the $p(2\times2)$ structure one may introduce four sublattices denoted as X_1, X_2, Y_1, and Y_2 in Fig. 1. The structures X_1 and X_2 (as well as Y_1 and Y_2) can be transformed into each other by a translation for one lattice constant in the x direction. The transformations $X_1\leftrightarrow Y_1$ and $X_2\leftrightarrow Y_2$ need a translation along the y direction. *The main aspect of the model under consideration is that the atoms are allowed to jump for one lattice constant in the x direction only*. As a result, X_1 domains can be transformed into X_2 domains (the same is valid for the $Y_1\leftrightarrow Y_2$ transformations), but the transformation of X-type domains into Y-type ones is forbidden. Thus the four types of domains are split into two groups X and Y.

In order to reduce the number of model parameters and to emphasize the role of jump anisotropy, we assume below that interatomic interactions are isotropic and, moreover, we take $\varepsilon_1=\varepsilon_2=-\varepsilon_3=1$ for the sake of concreteness.

In the present work we utilize two approaches for the investigation of model kinetics. The first one is based on Monte Carlo (MC) simulation of the lattice-gas model, where the system is characterized by the discrete lattice variable $\mathcal{C}(\vec{r})$ $[\vec{r}=(x,y),\ x=1,\ldots,X_{\max},\ y=1,\ldots,Y_{\max},\ X_{\max}Y_{\max}=\mathcal{M}]$, which takes two values, $\mathcal{C}(\vec{r})=0$ for an empty site and $\mathcal{C}(\vec{r})=1$ if the site is occupied. The system is then allowed to evolve, starting from an initial disordered state, according to the standard Metropolis algorithm with

periodic boundary conditions. Time in this case is measured in MC steps per atom.

The second approach is based on the mean-field (MF) analog of the 2D lattice-gas model, where instead of the discrete variable $\mathcal{C}(\vec{r})$ we use the continuous ''concentration'' $c(\vec{r})$ $[0\leqslant c(\vec{r})\leqslant 1]$ which may be treated as the occupation probability of an atom at the site $\vec{r}$. Such a model was used previously by Chen and Khachaturian[16] to study kinetics of phase transformation in intermetallics. The kinetics of this model is determined by the ''diffusion'' of the variable $c(\vec{r})$, and the evolution equation takes the Cahn-Hilliard form[1]

$$\dot{c}=\nabla L\nabla\frac{\delta\mathcal{F}[c]}{\delta c}, \tag{2}$$

where L is the ''mobility'' (in the general case it is a d-dimensional tensor). The mobility tensor has to be chosen according to the microscopic properties of the model. We have $L_{xy}=L_{yx}=0$ for symmetry reasons because diagonal jumps are not allowed. For the diagonal elements of the mobility tensor we took $L_{xx}=L_{yy}$ (chosen equal to 1, which defines a time scale) for the model of isotropic jumps and $L_{xx}=1$, $L_{yy}=0$ when only jumps in the x direction are allowed.

Equation (2) can be deduced from Fick's law $j=-L\nabla\mu$, where $\mu=\delta\mathcal{F}/\delta c$ is the chemical potential, combined with the continuity equation $\dot{c}+\nabla j=0$. Free energy functional in the MF approximation takes the following form:

$$\mathcal{F}[c]=\frac{1}{2}\sum_{\vec{r},\vec{r}'}\varepsilon(\vec{r}-\vec{r}')c(\vec{r})c(\vec{r}')+T\sum_{\vec{r}'}[c(\vec{r}')\ln c(\vec{r}')+(1-c(\vec{r}'))\ln(1-c(\vec{r}'))], \tag{3}$$

where $\varepsilon(\vec{r}-\vec{r}')$ is the interaction energy of atoms at the sites $\vec{r}$ and $\vec{r}'$. The evolution equation (2) now can be rewritten as

$$\frac{\partial c(\vec{r},t)}{\partial t}=(L_{xx}\nabla_x^2+L_{yy}\nabla_y^2)\times\left[\sum_{\vec{r}'}\varepsilon(\vec{r}-\vec{r}')c(\vec{r}')+T\ln\frac{c(\vec{r})}{1-c(\vec{r})}\right]. \tag{4}$$

To study the kinetics of the MF model, we solve Eq. (4) numerically for periodic boundary conditions with the explicit Euler method starting from a disordered initial state $c(\vec{r},0)=\theta+\delta c(\vec{r})$, where $\delta c(\vec{r})$ is a random perturbation with the mean magnitude of 0.1θ. We performed calculations for time up to $t_{\max}=600$ (time in MF calculation is measured in dimensionless units) and averaged over runs started with different initial disordered configurations. Notice that the MF kinetics is completely deterministic; the temperature variable T in Eq. (3) determines the shape of the free-energy surface, and the randomness is introduced by the initial configuration.

The structure of the $p(2\times 2)$ phase can be described as the product of static concentration waves[16] with wave vectors $\vec{k}_1=2\pi(\frac{1}{2},0)$ and $\vec{k}_1'=2\pi(0,\frac{1}{2})$ [the wave vector is defined as $\vec{k}=2\pi(x/X_{\max},y/Y_{\max})$],

$$c(\vec{r})=\theta[1+\phi_x\cos(\vec{k}_1\vec{r})][1+\phi_y\cos(\vec{k}_1'\vec{r})], \tag{5}$$

where ϕ_x and ϕ_y are two components of the order parameter $\vec{\phi}=(\phi_x,\phi_y)$, so that the completely ordered domains of the X_1, X_2, Y_1, and Y_2 types of the p(2×2) phase have the (ϕ_x,ϕ_y) values equal to $(1,1)$, $(-1,1)$, $(1,-1)$, and $(-1,-1)$, correspondingly. Substituting Eq. (5) into Eq. (3), we obtain the following expression for the free energy:

$$\begin{aligned}F(\phi_x,\phi_y;\theta,T)&=\mathcal{M}\Big\{\frac{\theta^2}{2}[V(0)+\phi_x^2V(\vec{k}_1)+\phi_y^2V(\vec{k}_1')+(\phi_x\phi_y)^2\\&\times V(\vec{k}_1+\vec{k}_1')]+\frac{T}{4}[s(\theta(1+\phi_x)(1+\phi_y))\\&+s(\theta(1+\phi_x)(1-\phi_y))+s(\theta(1-\phi_x)(1+\phi_y))\\&+s(\theta(1-\phi_x)(1-\phi_y))]\Big\},\end{aligned} \tag{6}$$

where $V(\vec{k})$ is the Fourier transform of the interaction energy $\varepsilon(\vec{r})$, and $s(y)=y\ln(y)+(1-y)\ln(1-y)$. For our choice of the interactions $(\varepsilon_1=\varepsilon_2=-\varepsilon_3=1)$ we have $V(0)=4$, $V(\vec{k}_1)=V(\vec{k}_1')=-8$, and $V(\vec{k}_1+\vec{k}_1')=-4$. Because $V(\vec{k})$ reaches its minima at the points $\vec{k}_1$, $\vec{k}_1'$, and $\vec{k}_2=\vec{k}_1+\vec{k}_1'$, the $p(2\times 2)$ structure provides the absolute minimum of the free energy of the system at coverages $\theta\leqslant\frac{1}{4}$. The equation for the curve which defines the order-disorder transition can easily be obtained from Eq. (6) by zeroing the second derivative of $F(\phi_x,\phi_y)$ over ϕ_x and ϕ_y at the point $\vec{\phi}=(0,0)$. The result is

$$T_c=|V(\vec{k}_1)|\,\theta(1-\theta)=8\,\theta(1-\theta). \tag{7}$$

Thus, for the coverages of interest in the present work, we have $T_c=1.5$ for $\theta=0.250$ and $T_c=0.875$ for $\theta=0.125$.

Considering the system defined above at a scale of the $p(2\times 2)$ unit cell, it is suitable to introduce the order parameter $\vec{\phi}(\vec{r})=(\phi_x,\phi_y)$ in terms of partial concentrations at the sites X_1, X_2, Y_1, and Y_2 as

$$\begin{aligned}\phi_x&=c_{X_1}-c_{X_2}+c_{Y_1}-c_{Y_2},\\\phi_y&=c_{X_1}+c_{X_2}-c_{Y_1}-c_{Y_2}.\end{aligned} \tag{8}$$

The characteristic length for the growth of domains is usually extracted from the analyses of the structure factor

$$S(\vec{k},t)=\left\langle\left|\mathcal{M}^{-1}\sum_{\vec{r}}[c(\vec{r},t)-\theta]\exp(i\vec{k}\cdot\vec{r})\right|^2\right\rangle, \tag{9}$$

where $\langle\ \rangle$ stands for the average over independent runs (ensemble average). However, for the highly anisotropic model that we consider here, it is important to study separately the characteristic lenghts for the two components $\phi_x(\vec{r})$ and $\phi_y(\vec{r})$ of the order parameter. According to Eq. (8) we can

calculate $\phi_x(\vec{r})$ and $\phi_y(\vec{r})$ at the scale of the $p(2\times2)$ unit cell, i.e., in a coarse-grained lattice which has half the initial number of cells in each direction. Then we calculate the correlation function $C_\phi(\vec{r},t)=\langle\phi(\vec{r},t)\phi(0,t)\rangle$ and its Fourier transform $S_\phi(\vec{k},t)$ for $\phi_x(\vec{r})$ and $\phi_y(\vec{r})$ separately. These quantities are then used to determine the characteristic lengths of interest as explained below for the jump-isotropic case (Sec. IV A) and the anisotropic case (Sec. IV B3).

III. PHENOMENOLOGICAL APPROACH

Before analyzing simulation results, let us briefly outline the predictions expected from a phenomenological approach.

In the model of isotropic jumps none of the components ϕ_x and ϕ_y of the $p(2\times2)$ phase order parameter is conserved [although the total concentration $c(\vec{r})$ is conserved]. All types of boundaries between different $p(2\times2)$ domains can be shifted by a jump of a single atom for one lattice constant in any direction. The motion of such walls is to be purely curvature driven, and the growth kinetics at late times should follow the ''fast'' Lifshitz-Allen-Cahn growth law $R(t)\propto t^{1/2}$.

By contrast, the model of anisotropic jumps puts an additional constraint on the component ϕ_y of the order parameter. Indeed, because transitions between X and Y sublattices are forbidden, ϕ_y must be conserved during system evolution, while ϕ_x is still a nonconserved quantity. Therefore, one may expect that time evolution of the ϕ_y component will be significantly slower than that of the ϕ_x component.

The model of anisotropic jumps has two different types of domain walls (DW's). The first type is the $X_1|X_2$ or $Y_1|Y_2$ wall which corresponds to the change of the ''fast'' component ϕ_x from $+1$ to -1. Such a wall can be shifted by a jump of a single atom for one lattice constant in the x direction. The dynamics of these walls has to be described by the ''fast'' growth law $R(t)\propto t^{1/2}$, similarly to the jump-isotropic model. The second type of DW is the $X|Y$ wall, which separates domains with opposite values of the ''slow'' component ϕ_y of order parameter. In the jump-anisotropic model the $X|Y$ wall cannot be shifted by an ordinary mechanism of a single-atomic jump. To shift the $X|Y$ wall, an atom of, say, the X domain must cross the area occupied by the Y domain, and then join any other X domain. Therefore, the growth mechanism necessarily involves long-range diffusion process through the body of the ordered phase. This has to lead to a strong slowing down of the growth, and the ''slow'' Lifshits-Slyozov growth law $R(t)\propto t^{1/3}$ is expected to apply at $t\to\infty$.[17]

Thus, the jump-anisotropic model is characterized by a hierarchy of growth rates due to different evolution of two components of the vector order parameter of the rarefied $p(2\times2)$ phase.

In addition, the dependence of the growth rate of the ordered phase on the atomic concentration has to be different for isotropic and anisotropic models. First, let us consider the model of isotropic jumps. For a concentration below the stoichiometric value $\theta_s=\frac{1}{4}$, the domains of the $p(2\times2)$ structure coexist with the lattice-gas phase. At early stages of evolution the $p(2\times2)$ domains grow independently from each other, taking atoms from a surrounding ''gas'' phase. Therefore, their growth should follow the ''fast'' law $R(t)\propto t^{1/2}$ up to some transient time t_c, and only at later times $t>t_c$ the ''gas'' phase becomes exhausted and the system passes to the coarsening stage. At this late stage the growth proceeds by the exchange of atoms between $p(2\times2)$ islands through the lattice-gas phase and, therefore, time evolution has to follow the ''slow'' Lifshits-Slyozov growth law $R(t)\propto t^{1/3}$. The crossover time t_c which separates the ''fast'' and ''slow'' growth kinetics, has to depend on the atomic concentration; that is, it has to vanish at low coverages, and has to be infinite for the stoichiometric concentration θ_s. Therefore, in the jump-isotropic model the most effective growth should be achieved at the stoichiometric concentration. The MC simulation data[15] are in agreement with this statement.

The behavior of the jump-anisotropic model, however, has to be more involved. Indeed, for the jump-anisotropic model at small θ, $\theta\ll\theta_s$, the growing islands are situated far from one another, and grow by an exchange of atoms through the lattice gas. Therefore we may expect that the model of anisotropic jumps will behave similarly to the isotropic model, i.e., the growth rate will increase with coverage at $\theta\ll\theta_s$. On the other hand, at higher coverages $\theta\sim\theta_s$, neighboring islands which belong to the different types X and Y start to overlap. The overlapping should decrease the growth rate, because the diffusion of atoms from the X island to another closest X island will proceed now not through the ''gas'' phase, but over a neighboring domain of the ''alien'' Y-type structure. Therefore the diffusing atom has to overcome an additional energetic barrier when entering the ''alien'' domain, and also the atomic diffusion within the alien structure should be much slower. For example, in the model under investigation the barrier for penetration is about 2ε, and the difference of activation energies for the atomic jump in the lattice gas and in the alien structure is about also 2ε, so the diffusion is slower by a factor of $\exp(-2\varepsilon/T)$. This impedes the growth rate at low temperatures significantly. Thus there is a concentration θ^* such that the growth rate increases with θ at $\theta<\theta^*$ but it decreases in the interval $\theta^*<\theta<\theta_s$, so that the growth rate has to have a maximum at $\theta\sim\theta^*$. Since the value θ^* corresponds to the situation when islands start to overlap for the first time, θ^* is to be coupled with the percolation threshold (which is about 0.5 for square lattices), and we obtain $\theta^*\approx0.5\theta_s=0.125$. The data of MC simulation[15] showed that the effective growth rate of the $p(2\times2)$ domains does exhibit a maximum at θ^*.

In the remainder of the paper we will combine the MC results with those for the MF model to test these predictions. The MF model provides a good qualitative picture for the growth mechanisms and exhibits well-defined DW's. The MC technique provides a more reliable quantitative description, and it can be applied at much lower temperatures, which are of prime interest in the present work.

IV. GROWTH KINETICS FOR A HOMOGENEOUS SYSTEM

A. Jump-isotropic model

Let us briefly illustrate here the behavior of the jump-isotropic model at the stoichiometric $\theta_s=0.250$ and half-

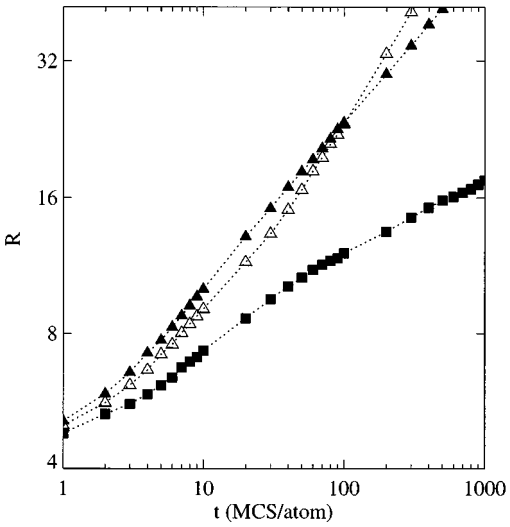

FIG. 2. Growth laws $R(t)$ for the model of isotropic jumps at $\theta=0.250$ (filled triangles) and $\theta=0.125$ (filled squares) at $T=0.33$. The $R(t)$ dependence for $T=0.77$ at $\theta=0.250$ is shown by open triangles.

stoichiometric $\theta=0.125$ concentrations in order to compare it later with the behavior of the jump-anisotropic model. We made series of 100 MC runs for a 128×128 lattice at low temperature $T=0.33$ (chosen as in Ref. 15). To determine the characteristic length $R(t)$ of the isotropic model, we used the following procedure. First, we calculated the structure factors $S_{\phi_x}(\vec{k},t)$ and $S_{\phi_y}(\vec{k},t)$ separately for both order parameter components ϕ_x and ϕ_y. Since we found no difference in their shapes and evolution, we calculated $S_\phi(k,t)$ as the average of $S_{\phi_x}(\vec{k},t)$ and $S_{\phi_y}(\vec{k},t)$ over ϕ_x and ϕ_y, and also over the x and y directions. Then we calculated the first moment $k^{\langle1\rangle}$ of the averaged structure factor $S_\phi(k,t)$, and determined the characteristic length $R(t)$ as $R=2\pi/k^{\langle1\rangle}$. Note that the values of $R(t)$ obtained in this way, coincide quite well with domain sizes seen in typical pattern pictures (see also the discussion of this question for the jump-anisotropic model below in Sec. IV B 3).

The log-log plots of $R(t)$ dependencies are shown in Fig. 2 [here and below, in all the figures with growth laws we consider only values of $R(t)$ which do not exceed one-third of the lattice size in order to avoid finite-size effects]. The slope of $R(t)$ at $\theta_s=0.250$ (Fig. 2, filled triangles) is $z\approx0.38$, and it is practically independent of time. By contrast, at a half-stoichiometric coverage $\theta=0.125$ (Fig. 2, filled squares) $R(t)$ tends to grow with the same exponent $z\approx0.38$ at early times $t<t_c\sim10$ Monte Carlo steps atom, while at later times the slope of $R(t)$ decreases, and growth proceeds further with a lower exponent $z\approx0.23$. The measured growth exponents are noticeably lower than the value $z=\frac{1}{2}$ expected for the stoichiometric coverage, as well as the value $z=\frac{1}{3}$ expected for late times $t>t_c$ in the nonstoichiometric coverage case. This points out a limitation of the numerical method to calculate exponents in a growth law. Accurate calculation of growth exponents in the asymptotic regime requires very long times and large systems. However, higher temperatures allow us to reach the asymptotic regime faster. the The simulation data for the temperature $T=0.77$

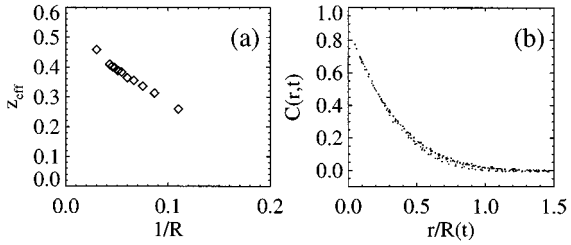

FIG. 3. Jump-isotropic model at $\theta=0.250$ and $T=0.77$: (a) finite time growth exponent vs $z_{\rm eff}$ $1/R$; (b) scaling of the normalized pair-correlation function $C(r,t)=C_\phi(r,t)/C_\phi(0,t)$ for $3<t<300$ MCS/atom.

and the concentration $\theta_s=0.250$, which are plotted in Fig. 2 by open triangles, show that the asymptotic growth with $z\approx\frac{1}{2}$ exponent is indeed achieved in the simulation. The corresponding finite time growth exponent $z_{\rm eff}$ (see Sec. IV B 4 below for details of $z_{\rm eff}$ determination) is shown in Fig. 3(a). The structure factor $S_\phi(\vec{k},t)$ as well as the correlation function $C_\phi(\vec{r},t)$ in the jump-isotropic model exhibit scaling, and have the shape typical of the case of a nonconserved order parameter [see in Fig. 3(b)].

Thus in the model of isotropic jumps the growth at half-stoichiometric coverage is much slower than at stoichiometric one. As we will see below, the behavior of the jump-anisotropic model is totally the opposite.

B. Jump-anisotropic model at stoichiometric concentration

We made a series of runs for the 128×128 lattice with both MC and MF techniques at the stoichiometric coverage $\theta=0.250$ and different temperatures. The results are the following.

1. Sequence of phase transformations in the MF model

First let us describe the sequence of phase transformations in the MF variant of the jump-anisotropic model at temperature $T=0.77$ which is below the critical temperature for both coverages $\theta=0.250$ and $\theta=0.125$ studied in the present work. Starting from $t\approx0.3$ we can observe a clear-cut $p(2\times1)$ modulation of $c(\vec{r})$ with $0<c(\vec{r})<0.5$ [Fig. 4(a)]. The $p(2\times1)$ modulation is oriented perpendicularly to the direction of atomic jumps, so that the peak of the structure factor $S(\vec{k})$ shows up at $\vec{k_1}=2\pi(\frac{1}{2},0)$. Two translational types of the $p(2\times1)$ regions are modulated in antiphase, and correspond to the opposite values of the ''fast'' component ϕ_x of the order parameter. During this early stage the system was observed to be homogeneous at the scale of (2×2) cell, and the $\phi_x=\pm1$ domains are characterized by an isotropic shape. To describe an average size of these domains we introduce a ''fast'' characteristic length $\tilde{R}(t)$.

At a time $t\approx4$ the system starts to decompose into comparatively large [several (2×2) cells in size] regions with reduced and increased local coverage. Simultaneously the formation of the $p(2\times2)$ structure is observed, manifesting itself in the development of a peak of the structure factor (9) near $\vec{k_1'}=2\pi(0,\frac{1}{2})$. The large $p(2\times1)$-modulated domains, formed at early stage, are decomposed at $t\approx4$ into a con-

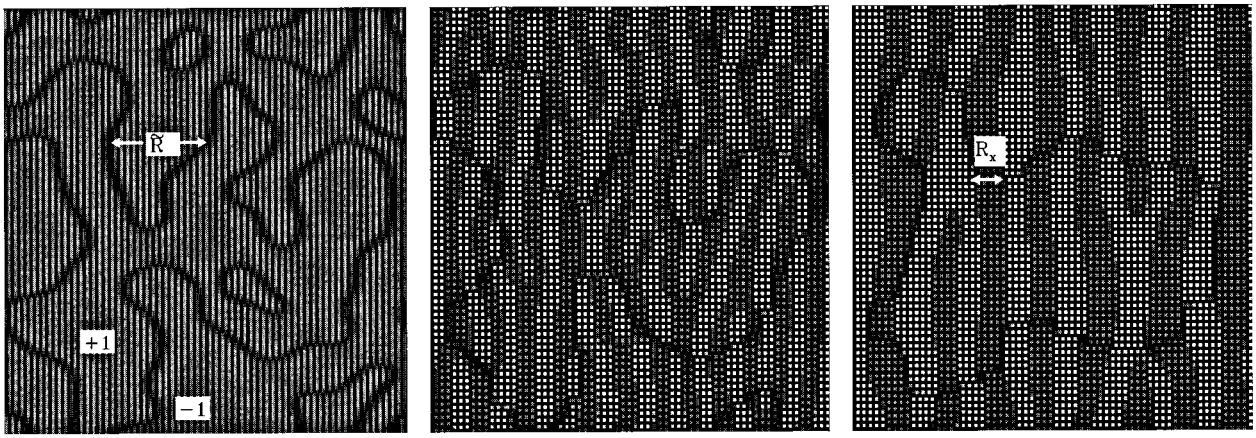

FIG. 4. Pattern evolution for the MF model of anisotropic jumps at stoichiometric coverage $\theta=0.250$ and $T=0.77$. Dark lattice sites correspond to $c(\vec{r})=0$, bright ones correspond to $c(\vec{r})=1$, and the grey scale describes intermediate occupation numbers. In the snapshots at $t=13$ and 130, in order to distinguish the X and Y domains, the brightness of the (say) X sites is artificially reduced by a factor of 2. Length scales $\tilde{R}$ and R_x are indicated with arrows.

figuration consisting of narrow alternating stripes with X_1 and Y_1 (or X_2 and Y_2) types of the $p(2\times2)$ structure, the stripes being oriented perpendicularly to the direction of atomic jumps [see Figs. 4(b) and (c)]. It is natural to associate the width R_x of these alternating stripes with the ''slow'' characteristic length scale of the jump-anisotropic model, connected with evolution of the ''slow'' order parameter component ϕ_y. Note that at $t\approx30$ the system again becomes almost homogeneous at the scale of the (2×2) cell.

Thus the typical pattern at a late stage of evolution of the jump-anisotropic MF model consists of large shape-isotropic domains of size $\tilde{R}$ which are characterized by a constant value of the ''fast'' order parameter component ϕ_x. These areas in turn are constructed of narrow X and Y alternating stripes of width R_x with opposite values of the ''slow'' order parameter component ϕ_y. Notice that such a configuration has predominantly domain walls of the $X|Y$ type.

2. Structure of domain walls

Let us dwell on the ''thin'' structure of the $X|Y$ domain walls in a more detail, because their motion determines late-stage kinetics of the model. Within a given $\phi_x=$const domain the $X|Y$ domain wall must be continuous owing to topological constraint; it may be broken at the $X_1|X_2$ (or $Y_1|Y_2$) boundary only. Therefore, all possible structural defects of the network of $X|Y$ domain walls are reduced to dislocations which we call *loops*. A loop may either be closed or it may have two free ends at the $X_1|X_2$ (or $Y_1|Y_2$), wall as is shown schematically in Fig. 5(a). The loops are the main objects that move at late stages of evolution of the jump-anisotropic model, because they have the largest curvature of DW's. The remainder of the $X|Y$ domain wall network is characterized by an almost zero curvature and therefore cannot move.

The growth of the R_x size of the stripelike structure proceeds according to the following mechanism: when a loop collapses (annihilates), the width of the current stripe increases with a factor of 3. Since the growth mechanism involves a long-range atomic diffusion through domains of alien structure, we may expect that the Lifshitz-Slyozov growth law will operate for R_x at $t\to\infty$. Simulation results indicate, however, that at finite times the growth proceeds with much lower effective exponent, as will be discussed in detail below in Sec. IV B 4.

Because loops play the main role in the growth process, it is important to consider possible sources of their formation. First, some loops exist from the very beginning of the evolution owing to the randomness of the initial configuration. Second, loops may emerge at ''fast'' $X_1|X_2$ (or $Y_1|Y_2$) boundaries which still exist even at late stages of evolution. However, at late times the fraction of ''fast'' boundaries becomes negligible compared with the fraction of ''slow'' $X|Y$ DW's, because $R_x/\tilde{R}\propto t^{1/3}/t^{1/2}=t^{-1/6}\to0$ when $t\to\infty$. Third, a loop may emerge inside the stripelike area, as shown schematically in Fig. 5(b). When two neighboring $X|Y$ and $Y|X$ domain walls meet each other at some point owing to a

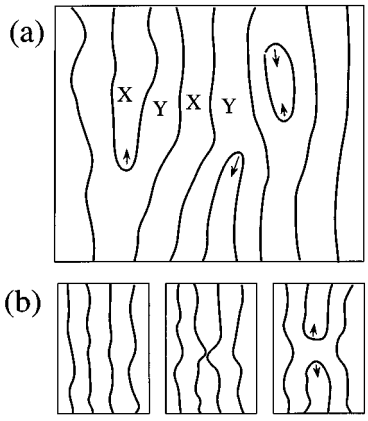

FIG. 5. (a) Sketch of the $X|Y$ domain walls structure in the model of anisotropic jumps. Main directions of loops motion are indicated by arrows. (b) Sketch of the creation of another pair of loops.

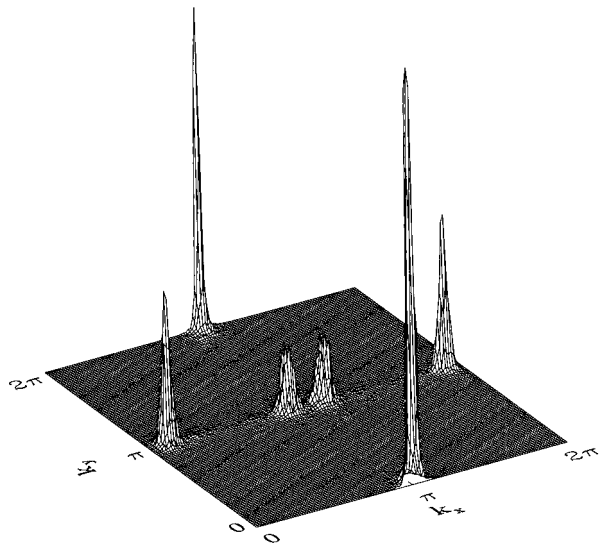

FIG. 6. Averaged structure factor $S(\vec{k})$ in the MF model of anisotropic jumps at $t=130$ and $T=0.77$.

large thermal fluctuation, they annihilate in the meeting area thus producing a pair of loops. The subsequent motion and disappearance of the newly produced loops result in an increase of R_x. To estimate a rate of loop creation, note that the formation of a pair of loops from the initially linear DW structure increases the total length of DW's by a value of order R_x [see Fig. 5(b)]. Therefore, the creation of a loop pair costs an energy of ΣR_x, where $\Sigma \sim |\varepsilon_3|$ is the DW energy per unit length. The probability of the loop-pair creation is thus $\exp(-\Sigma R_x/T)$, and the average time τ between these events is $\tau \sim \exp(\Sigma R_x/T)$. Inverting this expression, we obtain that this mechanism leads to the slow logarithmic increase of R_x as $R_x \sim (T/\Sigma)\ln t$.

A careful examination of typical patterns [as in Fig. 4(c)] shows that a $X|Y$ domain wall in average has a small deficit of atomic concentration comparing with the stoichiometric $p(2\times 2)$ coverage. As a result, the concentration profile in the x direction is slightly modulated with the period R_x. This concentration deficit may be explained in the following way. The energy of $X|Y$ domain wall with a width $\geqslant 2$ (recall that the lattice constant is taken as the unity of length) is equal to $|\varepsilon_3|/2$, while a narrower wall of the width of one lattice constant has a higher energy of $\varepsilon_2+|\varepsilon_3|/2$. Therefore, fluctuations of the DW width to higher values will be more probable than to smaller ones, and on average the DW width will be larger than two lattice constants.

3. Structure factor and length scales of the jump-anisotropic model

The structure factor (9) for the model of anisotropic jumps at $t=130$ [this time corresponds to the lattice pattern shown in Fig. 4(c)], averaged over ten independent runs, is shown in Fig. 6. One can see the difference in the shape of peaks around $\vec{k_1}=2\pi(\frac{1}{2},0)$ and $\vec{k_1}=2\pi(0,\frac{1}{2})$. The peak at $\vec{k_1}$, which is associated with the ϕ_x component of the order parameter, reaches its maximum exactly at the point $\vec{k_1}$, as it is typical for the nonconserved order parameter. By contrast, the peak around $\vec{k_1}=2\pi(0,\frac{1}{2})$, which corresponds to the ϕ_y component, splits into two subpeaks, and it has a zero intensity at the reference point $\vec{k_1}=2\pi(0,\frac{1}{2})$. The shape of this peak in the x direction looks similar to the typical shape of the structure factor in the case of a conserved order parameter.

As was shown above in Sec. IV B 1, the study of temporal evolution leads us to introduce at least two characteristic length scales for the model of anisotropic jumps. First, this model exhibits the ''fast'' length $\widetilde{R}$, associated with the isotropic evolution of the nonconserved component ϕ_x of the order parameter. Second, there exist the ''slow'' length scale introduced as the width R_x of the alternating X and Y stripes. This length scale is coupled to the evolution of the conserved component ϕ_y. In addition, since the shape of the stripelike domains with $\phi_y=\text{const}$ is strongly anisotropic, one has to consider their size R_y separately along the y direction (i.e., perpendicularly to the direction of atomic jumps). Notice that on the basis of our data we cannot give a clear answer whether R_y size evolves independently on R_x, or whether their evolution is coupled, and proceed with the same growth exponent z (although there are some reasons to believe that $R_y \propto R_x$; see Sec. IV B 4 below).

To extract all these quantities from the simulation data, we used the following procedure. First, for each run we calculated the structure factors $S_{\phi_x}(\vec{k},t)$ and $S_{\phi_y}(\vec{k},t)$ separately for ϕ_x and ϕ_y, as was described in Sec. II. Then we averaged the structure factors S_{ϕ_x} and S_{ϕ_y} over independent runs. The functions $S_{\phi_x}(\vec{k})$ and $S_{\phi_y}(\vec{k})$ look just like the peaks around $\vec{k_1}=2\pi(\frac{1}{2},0)$ and $\vec{k_1}=2\pi(0,\frac{1}{2})$ of the ''concentration'' structure factor (9), respectively (see Fig. 6). Although ''order-parameter'' structure factors $S_{\phi_x}(\vec{k})$ and $S_{\phi_y}(\vec{k})$ differ qualitatively by their shapes (thus reflecting different conservation conditions operating for the corresponding order-parameter components), in order to extract and compare different length scales $\widetilde{R}$, R_x, and R_y (as well as R for the jump-isotropic model), we have to elaborate a unique procedure for their calculation. This precludes a fitting by a given function as no predetermined shape would be suitable for all the curves to fit. Instead we have chosen a simple but reliable and commonly used probe: the calculation of the first moment of the structure factor in a given direction. To extract the ''fast'' length scale $\widetilde{R}$, we averaged the structure factor $S_{\phi_x}(\vec{k})$ over the x and y directions, because its evolution does not show any anisotropy. Then we calculated the first moment $k^{\langle 1\rangle}$ of the averaged structure factor, and obtained $\widetilde{R}=2\pi/k^{\langle 1\rangle}$. Analogously, the R_x value was determined as $R_x=2\pi/k_x^{\langle 1\rangle}$ where $k_x^{\langle 1\rangle}$ is the first moment of the structure factor $S_{\phi_y}(\vec{k})$ *along the x direction*. In addition, we determined the perpendicular R_y size of the $p(2\times 2)$ domains as $R_y=2\pi/k_y^{\langle 1\rangle}$ where $k_y^{\langle 1\rangle}$ is the first moment of the structure factor $S_{\phi_y}(\vec{k})$ *along the y direction* at $k=k_x^{\langle 1\rangle}$ It should be noted that according to this procedure, there is some subtle distinction in the interpretation of $\widetilde{R}$ and R_x, because $\widetilde{R}$ is related to the ''width'' of corresponding peak, while R_x contains the information about the ''split'' of peak

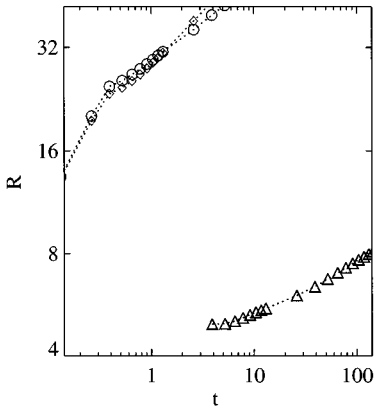

FIG. 7. Growth laws $\widetilde{R}(t)$ (circles) and $R_x(t)$ (triangles) for the MF anisotropic model at $\theta=0.250$ and $T=0.77$. The $R(t)$ dependence for the model of isotropic jumps is shown by diamonds.

in the x direction, i.e., its displacement with respect to $\vec{k}_1'=2\pi(0,\frac{1}{2})$. Nevertheless, we believe that all the extracted length scales can be correctly compared, because they fairly well coincide with real-space sizes estimated directly from the lattice patterns. This can be seen, for instance, by comparing the $\widetilde{R}$ and R_x values from first moments of the corresponding structure factors (Fig. 7) with the similar quantities, indicated with arrows in the snapshots (Fig. 4).

4. Domain growth in the jump-anisotropic model

Time dependencies $\widetilde{R}(t)$ and $R_x(t)$ for $\theta=0.250$, extracted from the series of ten MF runs for the 128×128 lattice at $T=0.77$, are plotted in Fig. 7. One can see that $\widetilde{R}(t)$ values are higher by an order of magnitude than $R_x(t)$. Note also that $\widetilde{R}$ is of the same order as the unique characteristic scale R of the *jump-isotropic model* for the same temperature (shown with diamonds in Fig. 7). However, it is too difficult to estimate the values of the growth exponents from the dependencies shown in Fig. 7 because the time intervals are too small. In order to obtain more reliable quantitative data, we made 50 MC runs for the same model parameters as in the MF runs (i.e. for 128×128 lattice, $\theta=0.250$, and $T=0.77$), and also 50 runs at much lower temperature $T=0.33$, used previously in Ref. 15. The time dependencies of $\widetilde{R}$ and R_x for the MC simulation are plotted in Fig. 8.

First, let us consider the data at higher $T=0.77$ (indicated with open symbols on Fig. 8). The values of the ''fast'' length scale $\widetilde{R}$ again generally resemble the $R(t)$ dependence for the model of isotropic jumps (Fig. 8, open diamonds), while the ''slow'' characteristic length R_x has much lower values. Also, in Fig. 8 we show with crosses the $R_y(t)$ dependence for this temperature. The uprising slope of all these curves indicate that the *finite time* growth exponent $z_{\rm eff}$ is increasing with time. But, to find the universality class of the system under study, we have to know the asymptotic ($t\to\infty$) growth exponent z. To do this, one can determine the finite time exponent $z_{\rm eff}$ using the formula

$$z_{\rm eff}=d(\ln R(t))/d(\ln t)\approx\log_{10}[R(10t)/R(t)], \qquad (10)$$

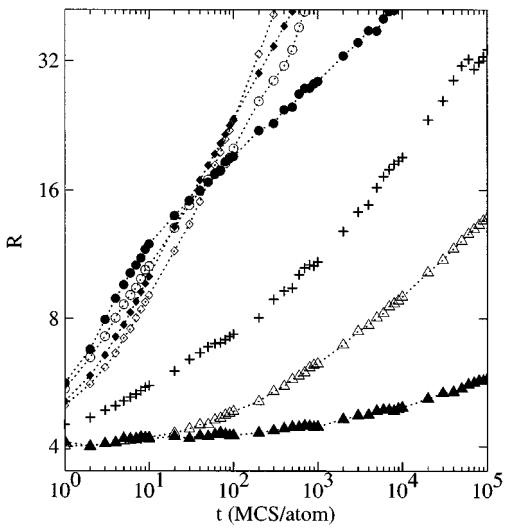

FIG. 8. Growth laws $\widetilde{R}(t)$ (circles) and $R_x(t)$ (triangles) for the MC simulation of jump-anisotropic model at $\theta=0.250$. The $R(t)$ dependencies for the jump-isotropic model at $\theta=0.250$ from Fig. 2 are replotted with diamonds for comparison. Data for $T=0.77$ with open symbols, data for $T=0.33$ are shown with filled symbols. The $R_y(t)$ dependence at $T=0.77$ is plotted with crosses.

and then extrapolate $z_{\rm eff}(1/R)$ dependence to $1/R\to0$. Note that, according to Ref. 5, the simplest finite time corrections to the growth exponent lead to the linear dependence $z_{\rm eff}=z-\alpha/R$. $z_{\rm eff}(1/R)$ for $\widetilde{R}(t)$ at $T=0.77$ is shown in Fig. 9(a), and the $z_{\rm eff}(1/R)$ dependencies for R_y and R_x are plotted in Figs. 10(a) and 10(b). Although our data are still very noisy, the extrapolations to $1/R\to0$ of the late-time part of the $z_{\rm eff}(1/R)$ dependence shown in Fig. 9(a) is in agreement with the Lifshitz-Allen-Cahn value $z=\frac{1}{2}$ for the ''fast'' characteristic scale $\widetilde{R}$. It is seen also, that the ''slow'' $R_y(t)$ dependence clearly exhibit the Lifshitz-Slyozov value of the asymptotic growth exponent $z=\frac{1}{3}$ [Fig. 10a)]. At the same time one can observe [Fig. 10(b)], that, for the ''slow'' R_x size, the finite time growth exponent $z_{\rm eff}(1/R)$ also tends to $z=\frac{1}{3}$ value at earlier times, while at later times the increase of $z_{\rm eff}$ with decreasing of $1/R$ is slower, so on the basis of our data for the asymptotic exponent z we cannot exclude a slightly lowered value in the interval $\frac{1}{4}<z<\frac{1}{3}$. In order to check if this lowering of the growth exponent is not related to finite-size effects, we made also 50 runs for the 128

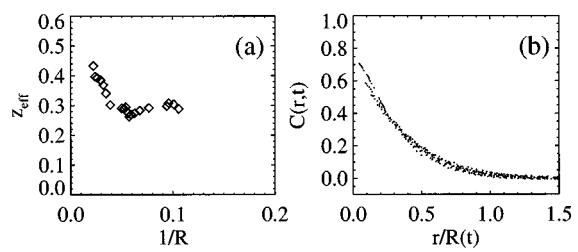

FIG. 9. ''Fast'' length scale $\widetilde{R}$ in the jump-anisotropic model at $\theta=0.250$ and $T=0.77$: (a) finite time growth exponent $z_{\rm eff}$ vs $1/\widetilde{R}$; (b) scaling of the normalized pair correlation function $C(r,t)=C_{\phi_x}(r,t)/C_{\phi_x}(0,t)$ for $3<t<700$ MCS/atom.

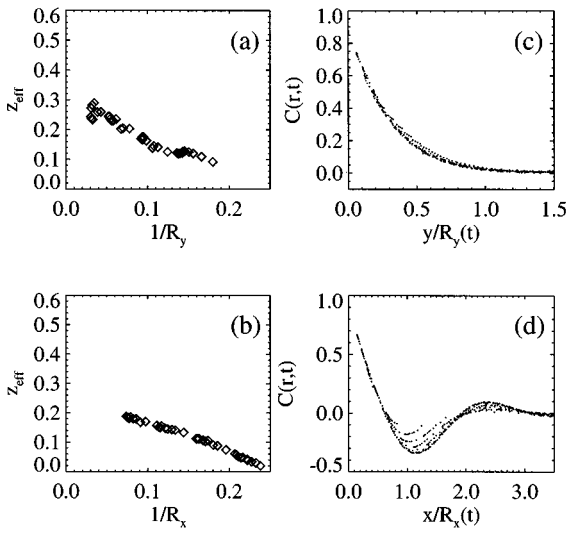

FIG. 10. ''Slow'' length scales $R_x(t)$ and $R_y(t)$ in the jump-anisotropic model at $\theta=0.250$ and $T=0.77$. Finite time growth exponent $z_{\rm eff}$ vs $1/R$ for $R_y(t)$ (a) and $R_x(t)$ (b). Scaling of the normalized pair-correlation function $C(r,t)=C_{\phi_y}(r,t)/C_{\phi_y}(0,t)$ for $10^2<t<10^5$ MCS/atom in the y direction (c) and in the x direction (d) (the depth of the minimum increases with time).

$\times 256$ and 128×32 lattices, and found no difference for growth law $R_x(t)$ in both these cases comparing with the results for 128×128 lattice. In any case, we note that generally these results are in quite good agreement with the predictions of Sec. III.

The scaling behavior of the correlation functions of the jump-anisotropic model is shown in Fig. 9(b) for $C_{\phi_x}(\vec{r},t)$ (the correlation function of the ''fast'' component ϕ_x), and in Figs. 10(c) and 10(d) for $C_{\phi_y}(\vec{r},t)$ (the correlation function of the ''slow'' component ϕ_y of the order parameter).

Now let us analyze the low temperature ($T=0.33$) data (Fig. 8, filled symbols). The evolution of both $\widetilde{R}(t)$ and $R_x(t)$ curves is much slower at this temperature. One can see that the slope of $\widetilde{R}(t)$ is even decreasing with time at $t>10$ MCS/atom. $R_x(t)$ stays almost constant up to $t\approx 10^3$ MCS/atom, and only later it starts to grow in some power-law fashion. Such a slow behavior can be explained, if one takes into account that the typical diffusion rate for an atom at $T=0.33$ is about 30 times lower than that at $T=0.77$, so the activated atomic jumps at low temperature $T=0.33$ can provide noticeable changes of R_x at much longer times only. Therefore, reliable determination of the asymptotic growth exponents at this temperature cannot be done on the basis of our data. We can only conclude, that at low temperature $T=0.33$ there exist a strong difference in the growth rates of the ''fast'' $\widetilde{R}(t)$ and ''slow'' $R_x(t)$ length scales.

5. Saturation effects in a finite-size system

The conclusions presented above are valid for an ideal infinite system only, while a real physical system always has a finite size l. The characteristic length l is usually determined by an average distance between defects such as, for instance, impurities and steps on crystal surfaces. In the classical jump-isotropic model the universal power-law growth $R(t)\propto t^z$ is valid as long as a domain size does not exceed the size of the system, i.e. for times $t<t^*$, where the ''saturation'' time t^* is determined by the relation $R(t^*)\sim l$. At later times $t>t^*$ the system reaches a glasslike state, where the ordering kinetics follows a logarithmic law, $R(t)\propto \ln t$.[18] The jump-anisotropic model should exhibit a similar behavior, but due to the hierarchy of growth rates, the saturation effects become more complicated. In this section we study the role of a finite size of the lattice.

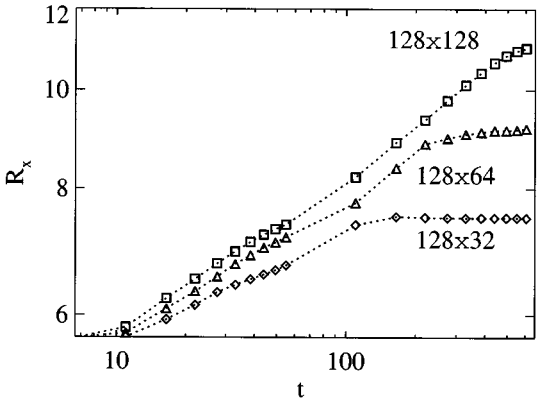

FIG. 11. Comparison of growth laws $R_x(t)$ for the MF anisotropic model at different $Y_{\max}$ sizes of the lattice at $\theta=0.250$.

As explained above in Sec. IV B 2, the power law for the growth of R_x is valid as long as the loops exist in the system. When the number of loops in the finite-size lattice is exhausted, the power-law growth should stop. Thus the MF model, where thermal fluctuations are absent and the only source of loops is the initial random configuration, should exhibit a ''saturation'' time t^* which has to depend on the lattice size. In order to test this assumption, we studied the time evolution for lattices with different sizes $Y_{\max}$ in the y direction. That is, we performed a series of ten runs in the framework of the MF model for 128×128, 128×64 and 128×32 lattices at the stoichiometric concentration $\theta=0.250$ at temperature $T=0.91$, which is still below the critical temperature at this coverage. The results for $R_x(t)$ are presented in Fig. 11. One can see that $R_x(t)$ exhibits a saturation time t^*, above which the average domain size R_x is practically constant and equal to some value R_x^*. Let us estimate the relation between $Y_{\max}$ and R_x^* The time t^* at which all the loops disappear within the finite area $X_{\max}Y_{\max}$, can be determined by the condition that the area occupied by a strongly anisotropic stripelike $p(2\times 2)$ domain is of the same order of magnitude as the area of the system, $X_{\max}Y_{\max}\sim R_x^*R_y^*$. Assuming that $R_y^*\propto R_x^*$ at late times, and $X_{\max}$ is kept fixed, we obtain, $R_x^*\propto\sqrt{Y_{\max}}$, which is in agreement with the data of Fig. 11.

Let us also briefly discuss the system evolution at $t>t^*$ in the presence of thermal noise. In this case the $X|Y$ DW's motion corresponds to its random walk, owing to thermal fluctuations. A further increase of R_x may now be governed by the thermal creation of pairs of loops inside the stripelike structure, as was discussed above in Sec. IV B 2. This mechanism should lead to the growth law $R_x\sim(T/\Sigma)\ln t$. It is remarkable that the parameters of this logarithmic growth for

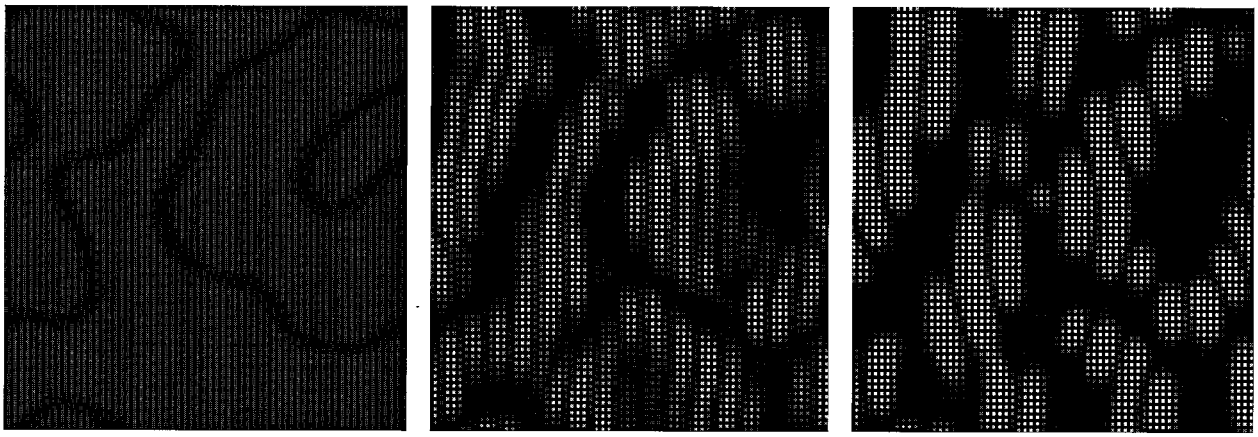

FIG. 12. Pattern evolution in the MF model of anisotropic jumps at half-stoichiometric coverage $\theta=0.125$ for $T=0.77$. The gray scale is mapped from $c(\vec{r})=0$ (dark) to $c(\vec{r})=1$ (white).

the model of anisotropic jumps are determined only by the internal energetic parameters of the model (by contrast with the conventional jump-isotropic case, where activation barriers should also depend on the characteristics of defects). It would be interesting in this connection to obtain evidence of such a logarithmic growth using the MC technique for a rectangular lattice with smaller $Y_{\max}$ size. Note that, as was mentioned above in Sec. IV B 4, at high temperature $T=0.77$ the power-law growth operates up to $t=10^5$ MCS/atom for a 128×32 lattice. We also made ten MC runs for the 128×32 lattice at lower temperature $T=0.33$ up to a much longer time $t=10^7$ MCS/atom. In this case we observed that at $t\approx2\times10^6$ MCS/atom the system crosses over to a slower behavior which is likely to be logarithmic. However, a very limited number of runs and a quite short available time interval for this slower growth did not allow us to determine its parameters reliably; that is why we do not present the corresponding picture here.

C. Jump-anisotropic model at half-stoichiometric concentration

The phenomenological approach of Sec. III, as well as the MC simulation,[15] suggest that in the jump-anisotropic model the most effective growth of the $p(2\times2)$ domains should take place at a coverage approximately half as low as the stoichiometric coverage $\theta=0.250$. Here we motivate this statement with the results of the MF model.

Typical stages of the evolution in the MF model at $\theta=0.125$ and $T=0.77$ are shown in Fig. 12. At the beginning, when the $p(2\times1)$ modulation of the system appears, the behavior is similar for both $\theta=0.250$ and 0.125 concentrations. However, the decomposition into regions with reduced and increased local concentration, and the formation of the $p(2\times2)$ domains, starts for $\theta=0.125$ at much later times (at $t\approx30$ versus $t\approx4$ for the stoichiometric coverage). Alternating X and Y $p(2\times2)$ stripes emerge from a $p(2\times1)$-modulated area within the regions with a higher local coverage, while the regions with lower coverage lose the $p(2\times1)$ modulation and become disordered. It is interesting to note that this disordering starts from the ''fast'' boundaries. The alternating X and Y stripes of the $p(2\times2)$ phase are formed within rather compact areas, and have a more isotropic shape than in the stoichiometric case [see Fig. 12(c)]. In such a configuration the fraction of boundaries with high curvature is much larger, than for the stoichiometric case, which should result in faster growth. ''Alien'' $p(2\times2)$ domains of X and Y types are separated by the surrounding disordered lattice-gas phase. This circumstance tends to increase the domain growth due to the faster diffusion in the lattice-gas phase, as was suggested in Sec. III.

To find the $R_x(t)$ dependence, we performed ten runs for a 128×128 lattice. The size R_x versus time t for the MF model at $\theta=0.125$ is plotted in Fig. 13 (a) in comparison with the $R_x(t)$ dependence for $\theta=0.250$ case. It is seen that the R_x values for the half-stoichiometric coverage are generally noticeably larger then those for the stoichiometric one. It is interesting to note also that the slope of the presented $R_x(t)$ dependence for $\theta=0.125$ is very close to $z=\frac{1}{3}$, unlike in the $\theta=0.250$ case, where this slope is much lower, $z\approx0.2$. This fact also coincides with the predictions of Sec. III, because asymptotic growth with the Lifshits-Slyozov ex-

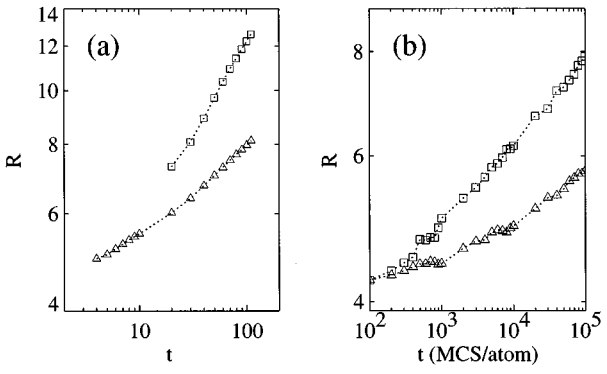

FIG. 13. Comparison of growth laws $R_x(t)$ in the model of anisotropic jumps at stoichiometric $\theta=0.250$ (triangles) and half-stoichiometric $\theta=0.125$ (squares) coverages. (a) MF results at $T=0.77$. (b) MC results at $T=0.33$.

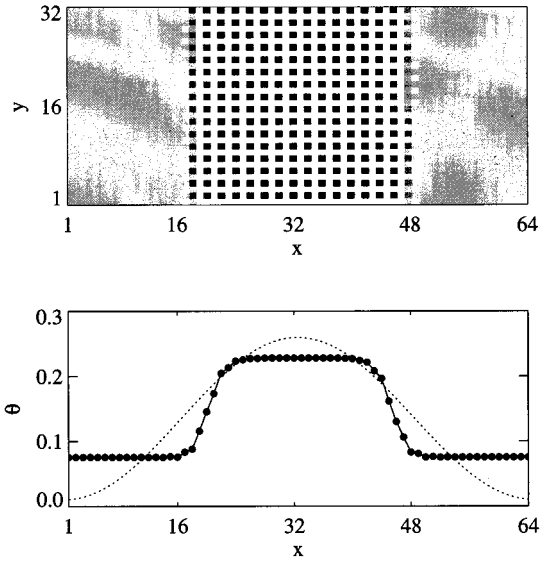

FIG. 14. Evolution of the nonuniform initial configuration in the framework of the MF model of isotropic jumps. The lattice pattern and corresponding coverage profile at $t=120$ are shown. The initial profile is marked with a dotted line. For a better view, the gray scale is mapped from $c(\vec{r})=0$ (white) to $c(\vec{r})=1$ (black), i.e., in the opposite direction, as in Figs. 4 and 12.

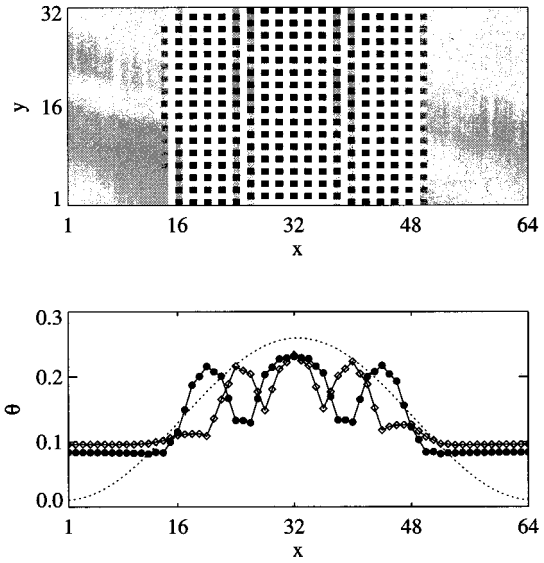

FIG. 15. Evolution of the nonuniform initial configuration in the framework of the MF model of anisotropic jumps. The lattice pattern at $t=120$ and coverage profiles at $t=30$ (diamonds) and $t=120$ (black circles) are shown. The initial profile is marked with a dotted line.

ponent $z=\frac{1}{3}$ for the $\theta=0.125$ case can be achieved at much earlier times due to faster diffusion of atoms in the lattice-gas phase, which occupies a large part of the surface at $\theta=0.125$.

Comparison of the MC simulation data at $\theta=0.250$ and coverages, extracted from the 20 MC runs for 128×128 lattice at much lower temperature $T=0.33$ [see. Fig. 13(b)], demonstrate a similar behavior, which is opposite to the behavior of the model of isotropic jumps (cf. with Fig. 2). Thus we conclude that the decrease of the coverage does lead to a faster growth of rarefied ordered domains in the system with anisotropic jumps.

V. EVOLUTION OF A CONCENTRATION GRADIENT

The aim of this section is to compare the kinetics of the jump-isotropic and jump-anisotropic models for the case when the initial configuration is not uniform, but has an initial concentration gradient. We simulated the system evolution starting with different nonuniform initial configurations, and using both the MF kinetic equation approach and the MC technique.

As shown above, the stripelike domains of the $p(2\times2)$ phase are rather stable well-defined objects at late stages of system evolution. In connection with this, an interesting question emerges about the character of the interaction between the neighboring X and Y ''alien'' domains. It is obvious that ''alien'' domains should repel each other. To study the character of this interaction, one should prepare a configuration where several stripes are formed compactly in some restricted area of the surface, but are then allowed to move to other parts of the surface. To realize such a situation in the MF case, we started from a sinusoidally shaped concentration in the x direction with $\theta_{\max}=0.27$, as shown in Fig. 14. This configuration is characterized by the mean coverage $\theta_{\text{mean}}=0.135$, which is well below the stoichiometric coverage. Since we were interested in the late-time behavior of several stripes only, we chose a rather narrow size of the lattice in the y direction. That is, we took the 64×32 lattice for both jump-isotropic and jump-anisotropic models.

MF simulation results at $T=0.83$ are presented in Figs. 14 and 15. One can see that the formation of the ordered phase begins in the region with increased concentration, while the rest of the surface acquires the disordered homogeneous state with the concentration $\theta\approx0.075$ which corresponds to the equilibrium lattice-gas phase at the chosen temperature. The behavior of the models of isotropic and anisotropic jumps shows a distinct difference. In the jump-isotropic model at early stage of evolution the continuous $p(2\times2)$ phase occupies a compact area with a well-defined boundary (see Fig. 14), and no further evolution of this configuration occurs. On the other hand, in the model of anisotropic jumps the alternating X and Y domains, formed at the beginning rather compactly within the center of initial distribution, later start to move away from each other (see Fig. 15). At the beginning of this process the $X|Y$ DW's are rather narrow and exhibit the clear-cut $p(2\times1)$ structure. However, later they became wider and more disordered. The local atomic concentration within the DW's decreases, so that the coverage profile acquires a nonmonotonic oscillating shape (see Fig. 15). In order to study the character of the domain motion, in Fig. 16 we plot the time dependencies of the width Δx of the region occupied by the $p(2\times2)$ phase (Δx was determined as the distance between left and right edges of corresponding coverage profiles in Figs. 14 and 15 at an arbitrary chosen level $\theta=0.16$). For the model of isotropic jumps this width is almost constant for all times $t\gtrsim10$, i.e., from the early stage of evolution (Fig. 16, triangles). A slight decrease of the width Δx with time is connected with the approaching of the stoichiometric coverage $\theta=0.250$ within the ordered

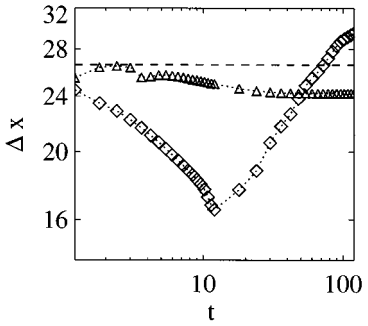

FIG. 16. The width Δx occupied by the $p(2\times2)$ phase vs time for the model of isotropic jumps (triangles) and the model of anisotropic jumps (diamonds).

area. By contrast, in the model of anisotropic jumps, after some initial decrease, the width Δx (Fig. 16, diamonds) starts to grow with time. The growth of the Δx is observed to follow a power law with an exponent close to $\frac{1}{3}$. This spreading of $p(2\times2)$ stripes is accompanied by the decrease of the mean coverage within the central Δx-area owing to the widening of the coverage-deficitable $X|Y$ DW's.

We made also several MC runs in both models of isotropic and anisotropic jumps for the 320×120 lattice with the random initial distribution of adatoms shaped as a narrow stripe of 80 lattice constants with the coverage $\theta_{\rm ini}\approx0.416$ (see Figs. 17 and 18), so that the mean coverage was $\theta_{\rm mean}\approx0.1$. The stripe was oriented perpendicularly to the x direction (the direction of atomic jumps in the jump-anisotropic model). The simulation temperature was chosen as $T=0.4$ which is well below T_c at $\theta_{\rm mean}\approx0.1$. The results are shown in Figs. 17 and 18 for both jump-isotropic and jump-anisotropic models, respectively. The coverage profiles in these figures were calculated by averaging the corresponding atomic configurations over two lattice constants in the x direction [i.e., over the $p(2\times2)$ period], and over the whole y size of the lattice.

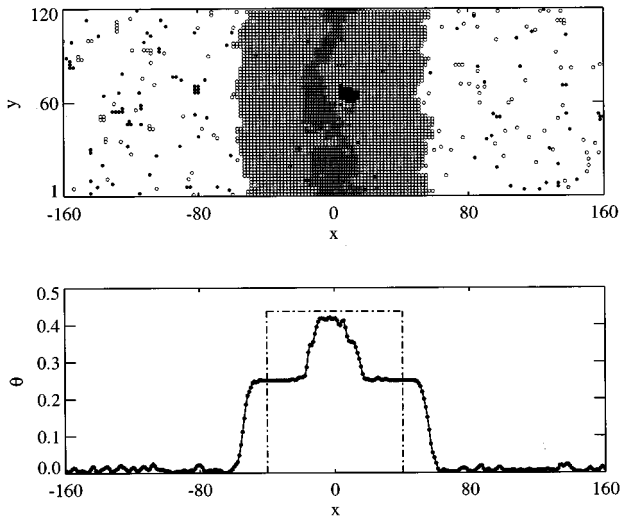

FIG. 17. Evolution of the coverage stripe in the model of isotropic jumps in the MC simulation. The lattice pattern and the corresponding coverage profile at $t=10^5$ MCS/atom are shown. The initial profile is marked with a dot-dashed line.

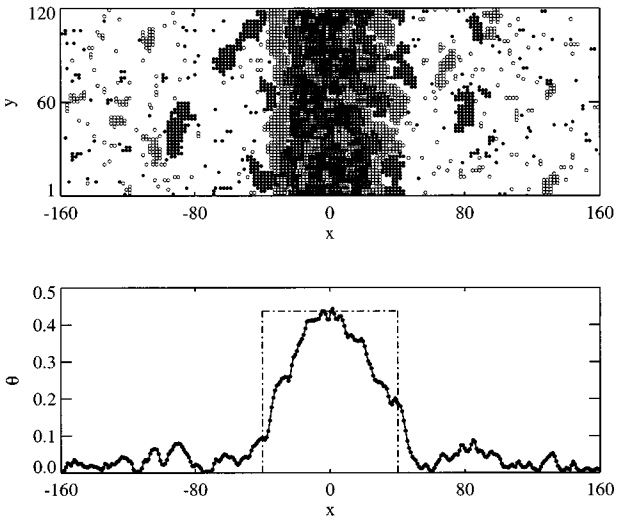

FIG. 18. Evolution of the coverage stripe in the model of anisotropic jumps in the MC simulation. The lattice pattern and the corresponding coverage profile at $t=9\times10^5$ MCS/atom are shown. The initial profile is marked with a dot-dashed line. In order to provide visual contrast between X and Y domains, atoms at the X and Y sublattices are indicated with open and filled symbols, respectively.

Similarly to the MF results, the *isotropic* case demonstrates the existence of a well-defined sharp solid-gas phase boundary corresponded to the first-order phase transition. Large compact domains of the $p(2\times2)$ phase are observed to form within the initial distribution. The formation of the $p(2\times2)$ phase manifests itself in the appearance of flat extended ''shoulders'' with $\theta\approx0.250$ on the concentration profile (see Fig. 17). The final configuration corresponds to a single compact $p(2\times2)$ domain surrounded by atoms in the disordered lattice-gas phase.

By contrast, the model of *anisotropic* jumps exhibits a quite unusual behavior. One can observe the peculiar process of pushing of strongly elongated $p(2\times2)$ islands outside the initial deposit, which then diffuse far away from the boundary into the lattice-gas phase (Fig. 18). The coverage profile is more smeared out, and it does not contain clear-cut terraces and drops. The escaped $p(2\times2)$ islands build up an extended concentration ''tail'' at the leading edge of the coverage profile. The average concentration in this tail is much smaller than the stoichiometric $\theta=0.250$ concentration. It is remarkable that the effective repulsion of the alien X and Y domains leads to the situation when an average distance between the $p(2\times2)$ domains within the tail is much larger than the radius of the interatomic interaction.

We observed also that the concentration in the ''tail'' for the jump-anisotropic model varies nonmonotonically with distance. At some distance from the initial boundary, where the growth rate of the ordered $p(2\times2)$ phase is expected to be higher than that for the stoichiometric coverage according to the results of Sec. IV C, one can see regions with local increase of the coverage. Although the averaging over statistically independent runs smears these nonmonotonities, we, nevertheless, may speculate (see below Sec. VI) that such a peculiar evolution of the concentration gradient in the jump-anisotropic model may manifest itself at a *macroscopic* scale

of time and distance in the formation of a *nonmonotonic* effective concentration profile.

VI. CONCLUSION

Thus we have shown that a strong anisotropy of atomic jumps in the 2D lattice-gas model, which has a degenerated rarefied ordered structure at low temperature, leads to the existence of two different types of domain walls characterized by different mechanisms of motion. In turn, this provides the existence of two characteristic length scales in the model, namely the ''fast'' and ''slow'' scales characterized by different growth laws.

The ''slow'' domain walls separate the ''alien'' X and Y types of the $p(2\times2)$ domains, differing by the vector of translation perpendicularly to the unique direction of atomic jumps and, therefore, these domains cannot be transformed into each other. This results in the formation of a specific stripelike superstructure of alternating X and Y domains, the period R_x of which grows with time according to the slow power law $R_x(t)\propto t^z$, with asymptotic growth exponent z close to the Lifshitz-Slyozov value $z=\frac{1}{3}$ (on the basis of our data we cannot exclude, however, a slightly lower value in the interval $\frac{1}{4}<z<\frac{1}{3}$). This slow growth is provided by the motion of the highly curved dislocations (loops) in an almost regular network of linearly shaped ''slow'' $X|Y$ domain walls.

We also demonstrated that decreasing the coverage below the stoichiometric value of the rarefied ordered phase leads to a faster domain growth. This situation differs from the conventional jump-isotropic case, where the maximum growth rate is reached at the stoichiometric coverage.

The above-described features of kinetics of the jump-anisotropic model reveal itself, in particular, in the character of the evolution of the concentration gradient. It was shown that the model of anisotropic jumps does not exhibit a sharp solid-gas phase boundary typical of the first-order phase transition in the conventional isotropic model. Instead, the repulsion of the ''alien'' ordered domains leads to their pushing into the gas phase and, consequently, to the smearing of the solid-gas boundary and to the formation of a long concentration tail with nonmonotonic ''humps.''

The proposed growth mechanism is quite general in the sense that it should be valid for any 2D lattice-gas model with a highly anisotropic mobility and the existence of a rarefied ordered phase with degenerated domains, characterized by the ''prohibition'' of the translation across the direction of atomic jumps. In this connection let us consider a possible application of the investigated model to the experimental result on a peculiar character of surface diffusion of lithium atoms on the furrowed Mo(112) surface at low coverages.[19] If we prepare an initial state, where the adatoms randomly occupy a half of the surface only (e.g., for $x\leqslant0$) with a coverage $\theta_{\rm ini}>\theta_s$, the step in the coverage will smooth out with time, but a phase transition occurring at θ_s has to manifest itself in the shape of the coverage tail $\theta(x)$ at $x>0$. At the first-order phase transition the chemical diffusion coefficient D falls to zero,[20] because at the transition point the equilibrium state corresponds to the coexistence of two phases. As a result, at some x^* the function $\theta(x)$ should exhibit a sharp drop from the ordered-phase coverage θ_s at $x<x^*$ to the value θ_g at $x>x^*$, where θ_g ($\theta_g<\theta_s$) corresponds to the lattice-gas phase (see Fig. 18). Notice that the tail function $\theta(x)$ decreases *monotonically* with x in this case.

However, in the experiment[19] a *nonmonotonic* Li concentration profile was observed in the course of diffusion out of the initial prepared step with $\theta_{\rm ini}\approx0.04$. The diffusion was investigated in the [111] direction, i.e., along the furrows of the Mo(112) surface. Two remarkable features were noted in the diffusion tail $\theta(x)$: *first*, the formation of the extended plateau at $\theta_s'\approx0.015$ probably corresponded to some rarefied 2D phase of lithium, and *second*, the shaping of the clear-cut ''hollow'' immediately behind the spreading plateau with the concentration $\theta'\sim0.5\theta_s'$ (for details see Ref. 19).

Here we suggest that the strong anisotropy of the Li-Mo(112) system [the ratio of Li diffusivity along and across the substrate furrows at low coverages is $10^3/10^4$ (Ref. 14)] plays a crucial role in such an unusual behavior of the Li film. Indeed, because in an anisotropic system the rate of growth of a rarefied phase as a function of the atomic concentration has a maximum at $\theta\approx0.5\theta_s$, the growth of islands of a rarefied ordered phase should proceed most effectively in the regions where the tail coverage is much lower than the stoichiometric one. We demonstrated that, due to the repulsion between the domains of the rarefied phase, an extended region consisting of widely spaced ordered domains does exist at the coverage profile $\theta(x)$ in the jump-anisotropic model (Fig. 18). Since on average the growth within this region is faster than at higher coverages, this may result, after a sufficiently long time of film evolution, i.e., at a *macroscopic* time and space scale, in the increase of the coverage at some distance away from the initial boundary. It is evident that the role of different surface defects should also be taken into account since (i) they can act as ''traps'' for moving islands, and (ii) they can change the ratio of atomic mobilities L_{xx}/L_{yy} for the anisotropic surface.

If the approach developed in the present work could be applied to the experiment,[19] the observed plateau should have a structure of θ_s islands separated by the lattice-gas phase. The ordered phase should correspond to a long-period rarefied structure of p($m\times m'$) type, with $mm'\sim50$. Interaction between adatoms which can provide the formation of such a rarefied structure does exist on anisotropic surfaces due to the competition between the dipole-dipole repulsive and the long-range oscillating indirect interaction of adatoms.[8] Low energy electron diffraction (LEED) experiments for the Li-Mo(112) adsystem (as well as for a number of other layers on the anisotropic surfaces[8]) showed that, along the furrows, the interaction is oscillating, and may exhibit a local minimum at distances at least up to nine lattice constants. So it is reasonable that a similar oscillating interaction may also exist in the direction across the furrows. Unfortunately, there are no reliable LEED experiments at coverages lower than $\theta\approx0.1$. However, the rarefied phase in the diffusional tail may in principle be observed by scanning tunnel microscope technique.

ACKNOWLEDGMENTS

We are indebted to T. Soboleva and A. Filippov for an illuminating discussion. O. M. B. thanks E. Majerníková for

the hospitality at Institute of Physics of Slovak Academy of Sciences, where a part of MC simulation had been performed. O. M. B. and M. V. P. were partially supported by Grant No. K5T100 from the Joint Fund of the International Science Foundation and the Government of Ukraine, and by NATO Linkage Grant No. LG 930236. M. V. P. highly acknowledges the warm hospitality of the Ecole Normale Supérieure de Lyon.

[1] J. D. Gunton, M. San Miguel, and P. S. Sahni, in *Phase Transitions and Critical Phenomena*, edited by C. Domb and J. L. Lebowitz (Academic, London, 1983), Vol. 8; K. Binder, Rep. Prog. Phys. **50**, 783 (1987); Z. W. Lai, G. F. Mazenko, and O. T. Valls, Phys. Rev. B **37**, 9481 (1988); O. G. Mouritsen, in *Kinetics of Ordering and Growth at Surfaces*, edited by M. G. Lagally (Plenum, New York, 1990), p.1; G. F. Mazenko, Phys. Rev. B **43**, 8204 (1991); A. J. Bray, Adv. Phys. **43**, 357 (1994).

[2] I. M. Lifshitz, Zh. Éksp. Teor. Fiz. **42**, 1354 (1962) [Sov. Phys. JETP **15**, 939 (1962)].

[3] S. M. Allen and J. W. Cahn, Acta Metall. **27**, 1085 (1979).

[4] I. M. Lifshitz and V. V. Slyozov, J. Phys. Chem. Solids **19**, 35 (1961).

[5] D. A. Huse, Phys. Rev. B **34**, 7845 (1986).

[6] T. M. Rogers, K. R. Elder, and R. C. Desai, Phys. Rev. B **37**, 9638 (1988); A. Chakrabarti, R. Toral, and J. D. Gunton, *ibid.* **39**, 4386 (1989).

[7] P. S. Sahni, G. S. Grest, and S. A. Safran, Phys. Rev. Lett. **50**, 60 (1983); K. Kaski, M. C. Yalabik, J. D. Gunton, and P. S. Sahni, Phys. Rev. B **28**, 5263 (1983); E. T. Gawlinski, M. Grant, J. D. Gunton, and K. Kaski, *ibid.* **31**, 281 (1985); J. G. Amar, F. E. Sullivan, and R. D. Mountain, two-dimensional *ibid.* **37**, 196 (1988).

[8] O. M. Braun and V. K. Medvedev, Usp. FIz. Nauk **157**, 631 (1989) [Sov. Phys. Usp. **32**, 328 (1989)].

[9] A. Sadiq and K. Binder, J. Stat. Phys. **35**, 517 (1984).

[10] A. Chakrabarti, J. B. Collins, and J. D. Gunton, Phys. Rev. B **38**, 6894 (1988); O. G. Mouritsen, P. J. Shah, and J. V. Andersen, *ibid.* **42**, 4506 (1990).

[11] T. Ala-Nissilä, J. D. Gunton, and K. Kaski, Phys. Rev. B **37**, 179 (1988).

[12] H. F. Poulsen, N. H. Andersen, J. V. Andersen, H. Bohr, and O. G. Mouritsen, Phys. Rev. Lett. **66**, 465 (1991).

[13] L. T. Wille, A. Berera, and D. de Fontaine, Phys. Rev. Lett. **60**, 1065 (1988).

[14] A. T. Loburets, A. G. Naumovets, M. V. Paliy, N. B. Senenko, and Yu. S. Vedula, Progr. Surf. Sci. **48**, 59 (1995).

[15] O. M. Braun and M. V. Paliy, Phys. Rev. Lett. **73**, 2091 (1994).

[16] Long-Qing Chen and A. G. Khachaturyan, Phys. Rev. B **44**, 4681 (1991); **46**, 5899 (1992);

[17] In the Ref. 15, for the long-time growth exponent we proposed the value $\frac{1}{5}$ on the basis of MC simulation data; however, we now realize that this it is not the case for the growth exponent at $t \to \infty$ (see details in Sec. IV B 4).

[18] D. A. Huse and C. Henley, Phys. Rev. Lett. **54**, 2708 (1985); G. S. Grest and D. J. Srolovitz, Phys. Rev. B **32**, 3014 (1985); D. Chowhury, M. Grant, and J. D. Gunton, *ibid.* **35**, 6792 (1987).

[19] A. G. Naumovets, M. V. Paliy, and Yu. S. Vedula, Phys. Rev. Lett. **71**, 105 (1993).

[20] L. A. Bolshov and M. S. Veschunov, Zh. Eksp. Teor. Fiz. **95**, 2039 (1989) [Sov. Phys. JETP **68**, 1179 (1989)].